Single Cigar-Shaped Nanopores Functionalized with Amphoteric Amino Acid Chains: Experimental and Theoretical Characterization

Mubarak Ali,[†,‡,*] Patricio Ramirez,[§] Hung Quoc Nguyen,[†,‡] Saima Nasir,[†,‡] Javier Cervera,[⊥] Salvador Mafe,[⊥] and Wolfgang Ensinger[†,‡]

[†]Department of Material- and Geo-Sciences, Materials Analysis, Technische Universität Darmstadt, D-64287 Darmstadt, Germany, [‡]GSI Helmholtzzentrum für Schwerionenforschung, D-64291, Darmstadt, Germany, [§]Departament de Física Aplicada, Universitat Politécnica de València, E-46022 València, Spain, and [⊥]Departament de Física de la Terra i Termodinàmica, Universitat de València, E-46100 Burjassot, Spain

ABSTRACT

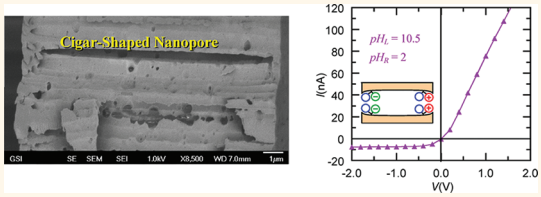

We present an experimental and theoretical characterization of single cigar-shaped nanopores with pH-responsive carboxylic acid and lysine chains functionalized on the pore surface. The nanopore characterization includes (i) optical images of the nanostructure obtained by FESEM; (ii) different chemical procedures for the nanopore preparation (etching time and functionalizations; pH and electrolyte concentration of the external solution) allowing externally tunable nanopore responses monitored by the current–voltage (*I*–*V*) curves; and (iii) transport simulations obtained with a multilayer nanopore model. We show that a single, approximately symmetric nanopore can be operated as a reconfigurable diode showing different rectifying behaviors by applying chemical and electrical signals. The remarkable characteristics of the new nanopore are the sharp response observed in the *I*–*V* curves, the improved tunability (with respect to previous designs of symmetric nanopores) which is achieved because of the direct external access to the nanostructure mouths, and the broad range of rectifying properties. The results concern both fundamental concepts useful for the understanding of transport processes in biological systems (ion channels) and applications relevant for tunable nanopore technology (information processing and drug controlled release).

KEYWORDS: cigar-shaped nanopore · amphoteric amino acid chains · current–voltage curves · logic functions

In living organisms, the ion channels of biological membranes[1,2] are responsible for the selective transport of chemical species across the cell membrane and the transfer of information in neural sensory networks. Most of these channels exploit the interaction between the charges fixed at the pore surface and the mobile ions in solution to process weak chemical and electrical signals in a noisy environment. When trying to design bioinspired devices that are capable of processing information on the basis of functionalized nanopores, a previous step to practical realizations is to identify what pore geometries and chemical functionalities are available to tune efficiently the nanopore characteristics by the application of external signals.

The control of predetermined nanopore geometries and surface functionalizations has now become possible.[3−14] The experimental procedures permit a variety of nanopore longitudinal shapes, including cylindrical, conical, double conical, concave pores with bullet-like tips, and convex pores with trumpet-like tips. Furthermore, different techniques, allowing for efficient control over the pore surface chemistry (and, in particular, of the fixed charge groups), have already been developed. To some extent, part of the biochemical diversity and functions of the ion channels inserted in cell membranes could be mimicked by nanostructures based on *asymmetric* pores with one type of electric charge, bipolar diodes and transistors composed by regions of different charge juxtaposed in series, and nanofluidic diodes with amphoteric chains functionalized on the pore surface.[3,4,15,16] Note also that single tracks constitute the elementary building blocks of the nanopore arrays typical of the membranes used for nanofiltration and protein separation, water desalination, biomolecule detection, controlled release of chemical drugs, and renewable energy storage.[9,17−19]

We provide here an experimental and theoretical characterization of approximately

* Address correspondence to m.ali@gsi.de.

Received for review March 7, 2012 and accepted March 29, 2012.

Published online March 29, 2012
10.1021/nn3010119

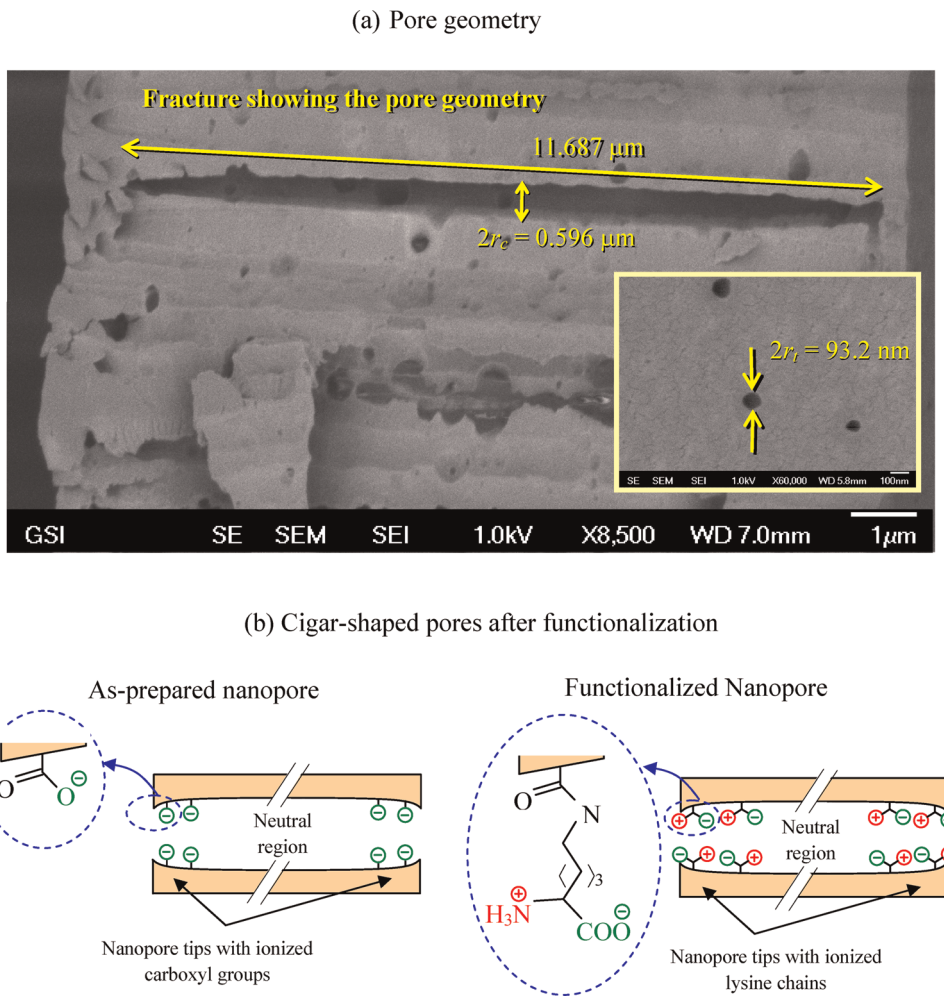

Figure 1. (a) FESEM images of approximately symmetric cigar-shaped nanopores. The fracture corresponds to a nanopore fabricated after 9 min of etching. The inset shows the tips of the nanopore obtained after 9 min of etching. Approximate values for representative central (r_c) and tip (r_t) nanopore radii are shown. (b) Sketch of the as-prepared (carboxylated) nanopores (not to scale) (left) and functionalized with lysine (right). Due to the geometry of the nanopore, the carboxylic and lysine groups are more concentrated close to the pore tips while the wide central pore region remains with a low surface density of functionalized groups.

symmetrical cigar-shaped nanopores. The nanostructures are obtained using the track-etching procedure,[6,17] leading to the generation of native chemical (carboxylic acid) groups onto the surface and inner pore walls. These groups are used for the attachment of amphoteric amino acid (lysine) chains onto the pore walls. The nanopore characterization involves field emission scanning electron microscopy (FESEM) imaging of the track-etched nanostructure, current−voltage (*I*−*V*) curves for different nanopore functionalizations, and transport simulations obtained with a multilayer membrane model. By manipulating the pH and electrolyte concentration of the external solution, a broad range of nanopore responses can be triggered. A single symmetrical nanopore can be operated as a multifunction reconfigurable diode by applying different external signals. The new nanopore characteristics include the sharp response observed in the *I*−*V* curves, the high external tunability provided by the convenient access to the pore mouths (the active nanopore layers here), and the broad range of rectifying properties that can be implemented. Potential applications concerning the implementation of logic functions and controlled release are finally suggested on the basis of the significant surface effects (electrical double layer phenomena) that result from the high surface/volume ratio typical characteristics of the nanopores.

Nanopore Characterization. *FESEM Imaging.* The FESEM images of Figure 1a show the fracture and the surface of the nanopores obtained in a polymer foil containing 5×10^7 pores/cm^2 approximately, which was etched simultaneously with the sample containing the single pore under the same conditions. The pore shapes of Figure 1a can be qualitatively explained by the hindrance effect caused by the surfactant-controlled diffusion, as described by Apel *et al.*[6,17] During the pore formation by the etching process, the surfactant molecules penetrate the pore tips, cover the walls,

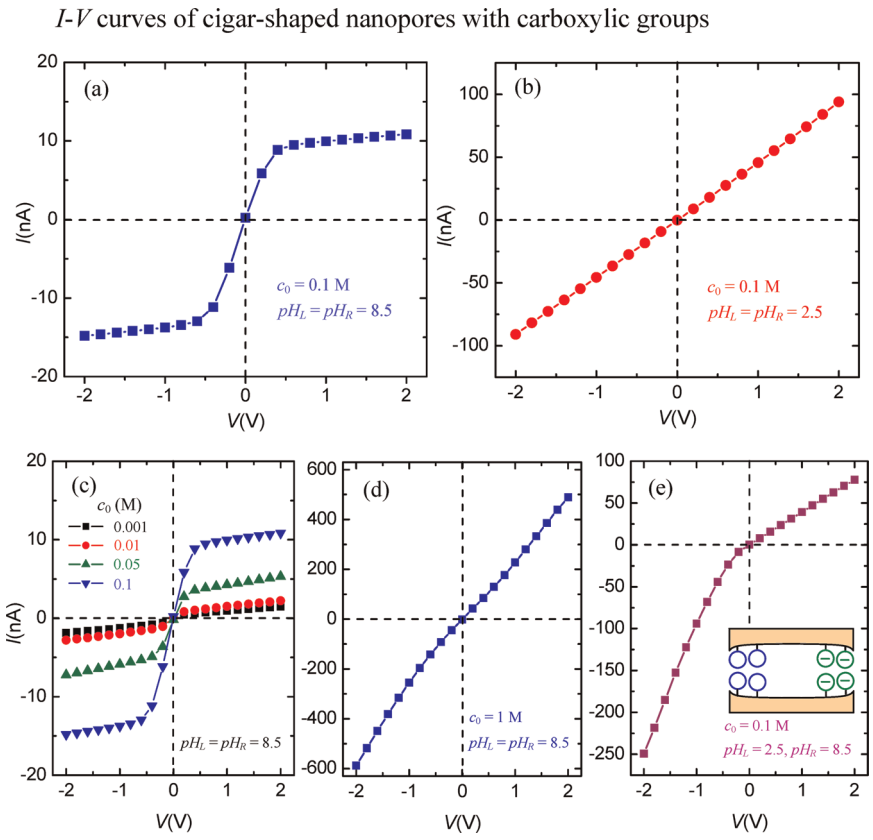

Figure 2. *I*–*V* curves of nanopores with carboxylic acid groups under different external conditions: (a) $c_0 = 0.1$ M, $pH_L = pH_R = 8.5$, current saturation; (b) $c_0 = 1$ M, $pH_L = pH_R = 2.5$, linear (ohmic) characteristics; (c) $pH_L = pH_R = 8.5$ parametrically in the electrolyte concentration, current saturation; (d) $c_0 = 1$ M, $pH_L = pH_R = 8.5$, quasi-linear (ohmic) characteristics; (e) acidic|neutral pH gradient, $pH_L = 2.5$ and $pH_R = 8.5$, diode-like characteristics with high (on) and low (off) conducting states. The estimated pore opening radius is 55 nm with an uncertainty of 5 nm.

and prevent further the diffusion into the central part of the pore because the adsorbed surfactant layer at the pore mouths leads a reduced permeability of the large molecules.[6] On the contrary, the small hydroxide ions are not blocked at the nanopore entrances and can proceed to the pore core. Therefore, the central pore diameter grows at a higher etching rate than the pore mouths, resulting in the cigar-shaped nanopore geometry shown in Figure 1a. By counting and taking the average sizes of more than 50 nanopores in the FESEM images, we obtained an average pore opening radius of 55 nm for the 9 min etching time nanopore and of 30 nm for the 6 min etching time nanopore, with an uncertainty of about 5 nm.

We will study the as-prepared nanopore containing carboxylic acid (COOH) groups, which are generated during the track-etching process, and pores modified with amphoteric amino acid (lysine) chains, as described in the Methods section. Schemes of the pores with the chemical functionalities are given in Figure 1b. We assume that the effect of the pore fixed charges is limited to the regions close to the narrow openings where the electrical double layer is formed, while this charge effect is negligible in the wide central region.

Current–*Voltage (I*–*V) Curves.* We consider now the experimental *I*–*V* curves of the nanopores before and after functionalization with amino acid (lysine) chains. In all cases, a polyethylene terephthalate (PET) foil of thickness $L = 12$ μm containing a single nanopore in the center separates two electrolyte (KCl) solutions of equal concentration c_0. The values pH_L and pH_R correspond to the left and right solutions, respectively. A potential difference (voltage) V is applied between the left solution and the right solution. The current $I > 0$ flows then from the left solution toward the right solution. Three pores were considered under different experimental conditions, and the resulting *I*–*V* curves are reported here and in the Supporting Information. Unless stated otherwise, the experimental data correspond to a nanopore with an etching time of 9 min. Decreasing this time to 6 min gives lower currents (see Supporting Information), probably because of the less developed openings of the resulting nanopore. Note that the electric current increases with the pore surface available for ionic transport.

The carboxylated (as-prepared) nanopore (Figure 2) shows the general characteristics of the nanopore. The sample containing this single pore was etched

simultaneously with a multipore membrane with an average pore opening radius of 55 nm and an uncertainty of 5 nm estimated from the FESEM images. The $I-V$ curve of Figure 2a corresponds to the case c_0 = 0.1 M and $pH_L = pH_R = 8.5$. At this pH value, the ionized carboxylate (COO^-) groups located at the two pore tips are negatively charged. The pore shows a quasi-symmetrical S-shaped $I-V$ curve, with a rapid current increase for low applied voltages (up to $|V| \sim 0.4-0.5$ V) followed by saturation at high V (above $|V| \sim 0.5$ V). Under basic conditions, the potential built up inside the negatively charged nanopore excludes the anions (Cl^-) in the electrolyte solution at the end pore constrictions, leading to current saturation because of the ion depletion phenomena that will be described in the next section. The $I-V$ curve of Figure 2b corresponds also to the symmetrical case c_0 = 0.1 M but now under acidic conditions. The quasi-linear curve demonstrates that the current saturation is absent when the nanopore tips become uncharged (at acidic pH values, the carboxylic acid groups are protonated and become neutral).

The $I-V$ curves of Figure 2c are parametric in the electrolyte concentration c_0 and show that the saturation current increases with c_0. This increase occurs up to a certain value of c_0 above which the current saturation effect is not observed. For the case c_0 = 1 M ($pH_L = pH_R = 8.5$), the nanopore exhibits quasi-linear $I-V$ characteristics (Figure 2d) because in concentrated electrolyte solutions the influence of pore fixed charges is negligible (the mobile carriers inside the pore effectively screen the fixed charges). The $I-V$ curve of Figure 2e corresponds to the asymmetric pH conditions ($pH_L = 2.5$ and $pH_R = 8.5$). The application of a pH gradient to the external solutions changes dramatically the $I-V$ characteristics that are now those of a nanofluidic diode showing current rectification. The applied pH difference forces the carboxylic acid groups close to the acidic solution to become protonated (neutral), while those close to the basic solution remain deprotonated (negatively charged). The pore shows then an asymmetric distribution of fixed charges, as schematically described in the inset of Figure 2e. There is a high conductance (on) state for $V < 0$ when the positive mobile carriers enter first the negatively charged tip and a low conductance (off) state for $V > 0$ when these carriers enter first the neutral tip. The pore diode with a junction between the charged region and the neutral region has been reported previously by Karnik *et al.*[20]

The experimental data of Figure 2 suggest that the $I-V$ characteristics of the as-prepared nanopore are dictated by the interaction of the mobile carriers with the fixed charges in the pore openings. Therefore, externally induced modifications in the charge distribution within the easily accessible pore tips can result in significant changes in the nanopore transport properties.

In order to gain more insight into the modulation of the ionic transport *via* the manipulation of the fixed charges located at the pore tips, we have studied the $I-V$ curves of the same nanopore after modification with lysine chains (Figure 1b, right). The results of Figure 3 have been obtained for c_0 = 0.1 M KCl, and the cartoons above the curves illustrate the charge state of the nanopore tips. Because of the amphoteric nature of the covalently tethered lysine chains, at strongly symmetric basic conditions ($pH_L = pH_R = 10.5$, Figure 3a), both amine (NH_2) and carboxyl (COO^-) groups are deprotonated and the net charge on the pore surface is negative. The nanopore is then selective to cations and shows current saturation, as observed in Figure 2a for the nanopores with ionized COO^- groups. At intermediate pH conditions ($pH_L = pH_R = 5$, Figure.3b), we are close to the lysine isoelectric point (pI = 5.6) where the amine (NH_3^+) groups are positively charged and the carboxyl (COO^-) groups are negatively charged. Therefore, the nanopore net charge is close to zero, and the $I-V$ curve shows a quasi-linear behavior. In strongly acidic conditions ($pH_L = pH_R = 2.5$, Figure 3c), both the amine (NH_3^+) and the carboxyl (COOH) groups are protonated. The positive charge on the pore surface provided by the NH_3^+ groups yields a nanopore selective to anions, and the $I-V$ curve displays again current saturation.

The curves of Figure 3d–f show diode-like $I-V$ characteristics with well-defined on and off conductance states due to the asymmetric fixed charge distributions generated by the applied pH gradients (see the cartoons above the curves). The case of $pH_L = 5$ and $pH_R = 10.5$ (Figure 3d) corresponds to a neutral|negative fixed charge distribution similar to that of the pristine nanopore under asymmetric pH conditions (Figure 2e). The pore is in the on state for $V < 0$ when the positive mobile ions enter first the pore tip with opposite fixed charges. Conversely, for $pH_L = 5$ and $pH_R = 2.5$ (Figure 3e), the fixed charge distribution is neutral|positive and the nanopore shows the on state when the negative mobile ions enter first the pore tip with positive fixed charges ($V > 0$). Finally, the case of $pH_L = 10.5$ and $pH_R = 2.5$ (Figure 3f) gives a negative|positive fixed charge distribution similar to that found in solid-state n–p diodes, bipolar ion-exchange membranes,[21,22] and conical nanopores with alternating regions of positive and negative fixed charges.[16,23,24] The resulting $I-V$ curve shows the on state for $V > 0$ when the negative and positive mobile ions enter first the respective pore tips with opposite fixed charges.

The rectification properties of asymmetric nanopores are characterized by the absolute value of the ratio r between the electric current in the on and off states at a given voltage. In the case of the neutral|negative and neutral|positive configurations of Figure 3d,e, the rectification ratios at $V = 2$ V are $r \sim 14$ and 9, respectively, while the negative|positive

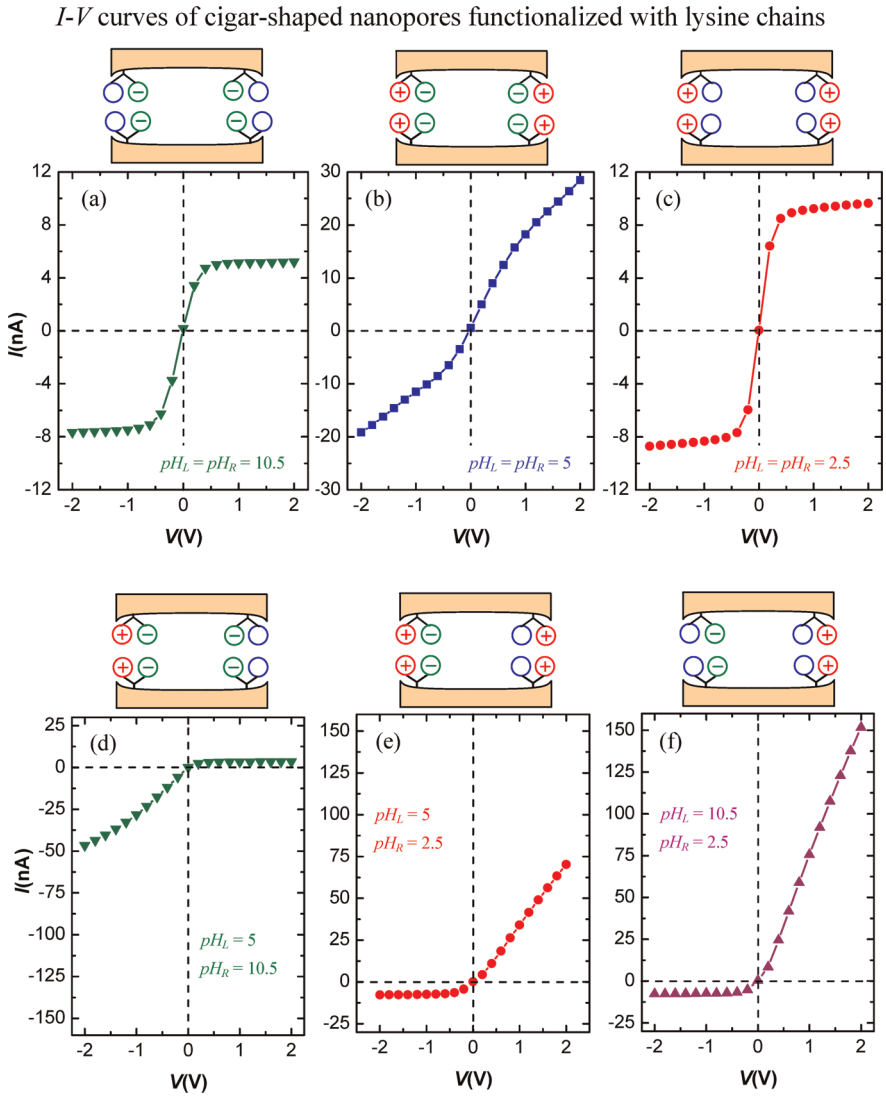

Figure 3. *I*−*V* **curves of nanopores functionalized with lysine chains at c_0 = 0.1 M and different pH conditions. Upper curves, symmetrical pH conditions: (a) basic medium, $pH_L = pH_R = 10.5$; (b) pH value close to the pI of lysine, $pH_L = pH_R = 5$; (c) acidic medium, $pH_L = pH_R = 2.5$. Lower curves, asymmetrical pH conditions: (d) pI|basic configuration, $pH_L = 5$ and $pH_R = 10.5$; (e) pI|acidic configuration, $pH_L = 5$ and $pH_R = 2.5$; (f) basic|acidic configuration, $pH_L = 10.5$ and $pH_R = 2.5$. The cartoons above each curve illustrate the distribution of fixed charges in the regions close to the pore tips. The nanopore is the same as that of Figure 2.**

configuration of Figure 3f yields $r \sim 20$ at the same voltage. This is in agreement with the experimental trends observed for conical nanopores functionalized with positive and negative charge regions juxtaposed in series.[16] The same finding was found by Nguyen *et al.*,[24] who have also shown the pH sensitivity of the system. The rectification ratios reported in this reference for bipolar conical pores are higher than those found here for the case of the cigar-shaped pore.

Higher values of r can be achieved by controlling the pore shape and charge distribution while keeping the pore openings constant.[12,14,15] In particular, the performance of the bipolar nanopore rectification could be improved by realizing a more abrupt junction between the positive and negative charge regions and by increasing the fixed charge concentration in these regions.[21−24]

The results of Figures 2 and 3 show some of the characteristics that could be expected in a cigar-shaped pore (this fact will be confirmed further in the Theoretical Model section). Additional experimental data for other pores concerning different sizes and etching conditions are presented in the Supporting Information. In conclusion, the experimental results of Figures 2 and 3 show that a broad range of rectifying properties can be implemented using a single reconfigurable nanostructure because of the easy external access to the pore mouths. This characteristic of the cigar-shaped pore is most desirable for practical applications.

Theoretical Modeling. *Model.* The pore shapes of Figure 1a give support to the theoretical model of Figure 4a composed by a core region of thickness d and radius r_c devoid of fixed charge groups surrounded by

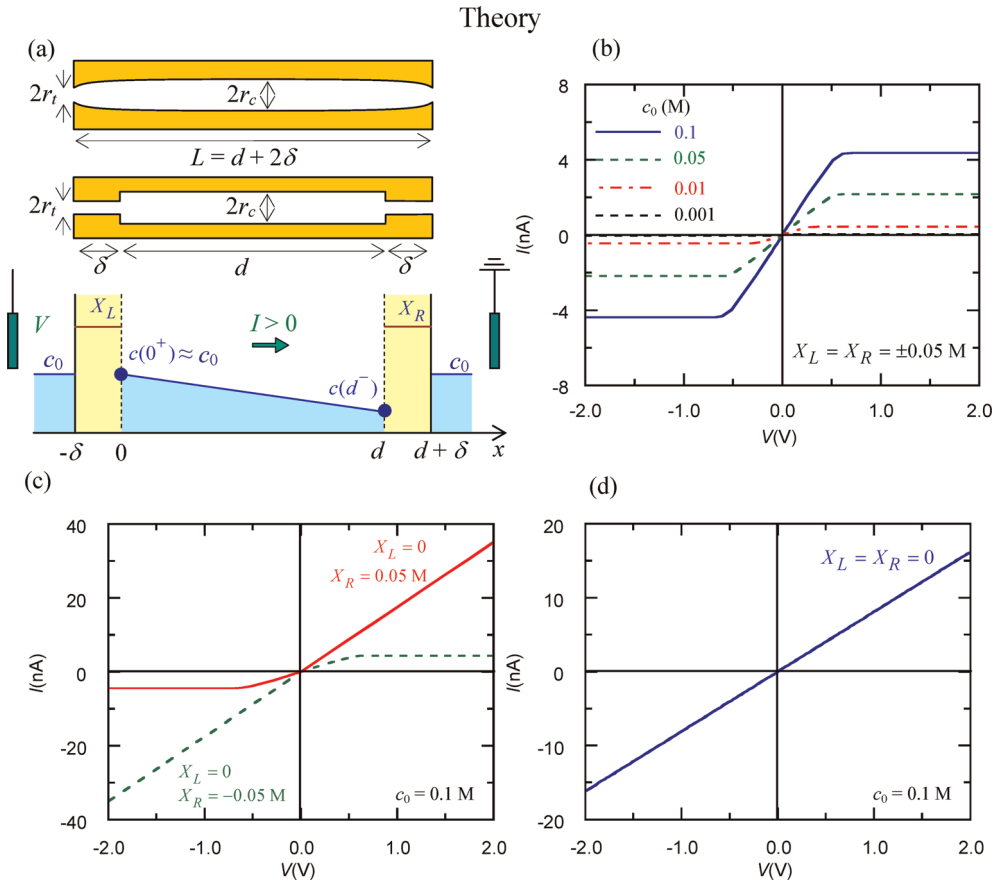

Figure 4. (a) Cigar-shaped nanopore is approximated by two charged regions (tips) of thickness δ and a central neutral region of thickness d. The sketch shows the mobile ion concentration profile across the neutral region of the multilayer model and the effective fixed charge concentrations X_L (left tip) and X_R (right tip). The sign criteria for the voltage V and the current I are also shown. (b–d) Theoretical I–V curves obtained for $c_0 = 0.1$ M and the following fixed charge concentrations (including the sign of the charge) $X_L = X_R \equiv X = \pm 0.05$ M (b); $X_L = 0$ and $X_R \equiv X = 0.05$ M (upper curve) and $X_L = 0$ and $X_R \equiv X = -0.05$ M (lower curve) (c); and $X_L = X_R = 0$ (d).

two step-like charged regions of thickness δ and effective radius r_t at the pore tips. While the transition between the regions may not be as sharp as assumed, the pictures of Figure 1a clearly show that two relatively narrow mouths are surrounding a relatively long and wide central core. The model assumed in Figure 4a is also in agreement with the schematic pore of Figure 3 in ref 6 that was suggested on the basis of a set of images showing typical cigar-shaped nanopores. The ratio between the mouth and central pore effective diameters depends on the particular etching conditions, the type of surfactant, and the etching time (see Supporting Information).[6,17] We will tentatively assume $r_t/r_c \approx 10$ and $\delta/d \approx 10$ as typical values in the model, in agreement with the dimensions of the pores shown in Figure 1a.

The distribution of fixed charges along the pore axis coordinate x and the local concentration $c(x)$ of electrolyte across the neutral core are also included in Figure 4a. The electrolyte depletion occurs close to $x = d$ for $I > 0$ and close to $x = 0$ for $I < 0$. In the two cases, we assume that the electrolyte concentration should be similar to the external concentration c_0 in the nondepleted region of the pore center, which corresponds to $x = 0$ for $I > 0$ in Figure 4a.

The steady-state ionic transport is governed by the one-dimensional Nernst-Planck equations[25–27]

$$J_i = -D_i\left(\frac{dc_i}{dx} + z_i c_i \frac{F}{RT}\frac{d\phi}{dx}\right) \quad (1)$$

the electroneutrality equation

$$\sum_i z_i c_i(x) + X_M(x) = 0 \quad (2)$$

and the continuity equation

$$\frac{dJ_i}{dx} = 0 \quad (3)$$

where J_i, D_i, $c_i(x)$, and z_i are the flux density, the diffusion coefficient, the local concentration, and the charge number of ion i. Also, $X_M(x)$ is the local concentration of fixed charges across the multilayer model of Figure 4a, F and R are the Faraday and universal gas constants, T is the absolute temperature, and $\phi(x)$ is the local electric potential.

In general, eqs 1–3 must be solved numerically. However, we will introduce now some plausible

simplifying assumptions that allow us to obtain analytical expressions for the $I-V$ curves as a function of the relevant experimental parameters. In the charged regions close to the pore tips, we approximate the counterion concentration by the absolute value of the respective fixed charge concentration, assuming then total co-ion exclusion. In the neutral core region, we write $i = F(J_+ - J_-)$ for the current density and use eq 3, together with the electroneutrality condition $c_+ = c_- \equiv c(x)$ (eq 2), to obtain $c(x) = c_0[1 - (i/i_L)(x/d)]$ for the electrolyte concentration profile (see Figure 4a), where the limiting current density is

$$i_L \equiv \frac{2FDc_0}{d} \quad (4)$$

and the two mobile species (K^+ and Cl^-) have the same diffusion coefficient D in aqueous solutions. The above linear profile for the electrolyte concentration permits one to evaluate readily the electrical resistance across the neutral region.[25] The total potential drop across the multilayer model of Figure 4a is then obtained by adding the resistances of the two fixed charge regions with constant mobile ion concentrations to the resistance of the neutral region.[13,21,25,27]

For the case $X_L = X_R \equiv X$, which corresponds to a central core surrounded by two charged regions with identical fixed charge density, the $I-V$ curve takes the form

$$\frac{FV}{RT} = \frac{2(A_c/A_t)(\delta/d)}{[1+(X/2c_0)^2]^{1/2}}\frac{I}{I_L} + \ln(1 + I/I_L),\ V < 0 \quad (5)$$

$$\frac{FV}{RT} = \frac{2(A_c/A_t)(\delta/d)}{[1+(X/2c_0)^2]^{1/2}}\frac{I}{I_L} - \ln(1 - I/I_L),\ V > 0 \quad (6)$$

where $A_c \equiv \pi r_c^2$ and $A_t \equiv \pi r_t^2$ are the cross-section areas of the core and tip regions, respectively, and $I_L \equiv A_c i_L$. Introducing these effective cross-section areas allows understanding qualitatively the change of the experimental currents with the nanopore etching time (see Supporting Information) because the pore surface available for ionic transport increases with this time. For $X_L \equiv X < 0$ and $X_R = 0$ (a central core surrounded by a negatively charged region on the left side and a neutral region on the right side; see Figure 4a), the $I-V$ curve is

$$\frac{FV}{RT} = \frac{(A_c/A_t)(\delta/d)}{[1+(X/2c_0)^2]^{1/2}}\frac{I}{I_L} + \frac{\delta}{d}\frac{A_c}{A_t}\frac{I}{I_L} + \ln(1 + I/I_L),\ V < 0 \quad (7)$$

$$\frac{FV}{RT} = \left\{\frac{(A_c/A_t)(\delta/d)}{[1+(X/2c_0)^2]^{1/2}} + 1 + \frac{\delta}{d}\frac{A_c}{A_t}\right\}\frac{I}{I_L},\ V > 0 \quad (8)$$

Finally, for $X_L = X_R = 0$ (a central core surrounded by two neutral regions). the $I-V$ curve simplifies to

$$\frac{FV}{RT} = \left(2\frac{\delta}{d}\frac{A_c}{A_t} + 1\right)\frac{I}{I_L} \quad (9)$$

RESULTS AND DISCUSSION

The results obtained with the theoretical model are shown in Figure 4b–d. In all cases, we have used c_0 = 0.1 M, $D = 2 \times 10^{-9}$ m^2/s, r_c = 600 nm, r_t = 60 nm, d = 10 μm, and δ = 1 μm as characteristic values for the electrolyte solution and nanopore dimensions of the experiments. The $I-V$ curves of Figure 4b correspond to the symmetrical case $X_L = X_R = \pm 0.05$ M (eqs 5 and 6) and can then be compared with the experimental data of Figure 2a,c (nanopore with carboxylic acid groups) and Figure 3a,c (nanopore with lysine groups). All of these experiments concern a nanopore with a central core surrounded by two regions with fixed charges of the same sign. For this symmetrical case, the model predicts S-shaped $I-V$ curves showing a rapid increase of the current with the voltage followed by current saturation at high voltage, as observed experimentally.

The current saturation regime occurs when the interfacial region between the central core and the fixed charge region at the right pore tip becomes depleted of mobile ions ($c(d^-) \approx 0$ in Figure 4a) at sufficiently high *positive* currents. This phenomenon is also characteristic of ion exchange membranes with (neutral) diffusion boundary layers.[25] Conversely, for high enough *negative* currents, it is the interface between the left fixed charge region and the central core region that is depleted of mobile ions ($c(0^+) \approx 0$ in Figure 4a). The experimental data are also in approximate agreement with the linear increase of the limiting current I_L with c_0 predicted by eq 4 (compare Figures 2c and 4b).

Figure 4c shows the theoretical $I-V$ curves in the cases $X_L = 0$ and $X_R \equiv X = 0.05$ M (upper curve) and $X_L = 0$ and $X_R \equiv X = -0.05$ M (lower curve) obtained with eqs 7 and 8. These curves can be compared now with those of Figure 2e (nanopore with carboxylic acid groups) and Figure 3d,e (nanopore with lysine groups). In these experiments, the nanopore has a neutral tip region, the central neutral core, and one charged tip region, all them juxtaposed in series. Again, the theoretical results reproduce the experimental trends observed. The $I-V$ curves show current rectification with well-defined on and off conductance states that are obtained for positive or negative voltages, depending on the sign of the fixed charges within the respective charged tip region. The limiting currents observed are due to the progressive depletion of mobile ions at the interfacial region between the central core and the charged tip region. In the case of the bipolar nanopore of Figure 3f), the rectification is more marked because of the enhanced conductance observed for $I > 0$.[21,22,28]

Finally, the theoretical $I-V$ curve for the case $X_L = X_R = 0$ is shown in Figure 4d. The linear behavior obtained can be compared to those observed for the neutral nanopores with carboxylic acid and functionalized lysine groups in Figures 2b,d and 3b. Because the three

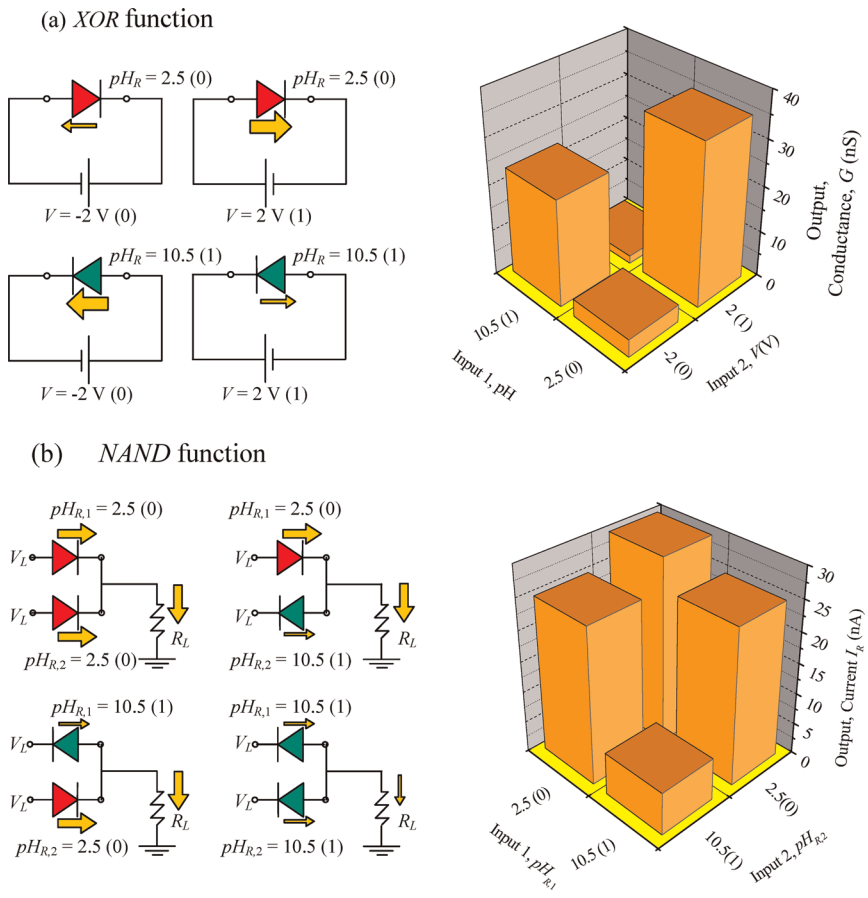

Figure 5. Implementation of logic functions XOR and NAND using nanopores functionalized with lysine. (a) Logic function XOR is based on a single nanopore. The inputs are the voltage *V* applied to the nanopore and the pH value of the right solution. The output is the nanopore conductance. (b) Logic function NAND is realized with a parallel arrangement of two nanopores connected in series to a resistance R_L = 50 MΩ. The inputs are the pH values in the respective nanopore right solutions, and the output is the current passing through resistance R_L. This current is obtained by solving the electrical circuit in each case. In the two logic function implementations pH_L = 5, c_0 = 0.1 M and the experimental nanopore conductances are taken from Figure 3d,e. The arrow size denotes the relative values of conductances (a) and currents (b).

pore regions are now approximately neutral, no depletion occurs in the vicinity of the tip|core and core|tip interfaces. As a result, no current saturation is observed and the pore behaves as an ohmic resistor.

The qualitative agreement between the theoretical results obtained with the model of Figure 4 and the experimental data of Figures 2 and 3 confirms that the continuum models can approximately describe the electrical interactions between the nanopore fixed charges and the mobile ions in the solution because the pore radii are much larger than the ionic size.[29,30] In a recent study on the effects of nanopore entrance on ion transport in nanochannels, Cheng and Guo[23] have also verified the validity of the continuum approach. This conclusion holds also for the case of wide pore ion channels like the porin OmpF (outer membrane protein F) found in the external membrane of bacteria *Escherichia coli* that can be engineered into a nanofluidic diode with pH-dependent electrical rectification.[2] In our case, a more detailed knowledge of the pore geometry and the distribution of fixed charges close to the pore tips could permit further refinements in the theoretical model to provide a quantitative description.

Logical Functions. The diode-like *I*−*V* curves of Figure 3d,e could be exploited to support logic functions that should be useful for nanofluidic chemical processors and actuators implemented using the pores functionalized with lysine chains. Previous theoretical and experimental schemes of logic functions at the nanoscale involve functionalized nanonoparticles arrays,[31] molecular arrays and self-assembled monolayers,[32] nanorod and nanowire devices,[33] and nanofluidic diodes.[3,4,15,34,35] Single cigar-shaped nanopores functionalized with lysine show a broad range of rectification properties that can be externally tuned, being ideal candidates to implement logic functions.

The two examples of Figure 5 correspond to the logic functions *XOR* (Figure 5a) and *NAND* (Figure 5b). The results are based on the modulation of the electrostatic interaction between the mobile ions and the electrically charged groups on the surface and inner nanopore walls. In both cases, the pH value of the left solution is fixed to pH_L = 5 and c_0 = 0.1 M. The XOR

function, which is usually difficult to implement with chemical systems, can be obtained here with a single nanopore. The first input signal is the voltage applied to the nanopore, $V = -2$ V (input 0) and $V = 2$ V (input 1). The second input signal is the pH value of the right solution, $pH_R = 2.5$ (input 0) and $pH_R = 10.5$ (input 1). The output is the nanopore conductance evaluated from the $I-V$ curve of Figure 3d,e (inputs 0 and 1 correspond to low and high conductance levels).

The NAND function is implemented with a parallel arrangement of two nanopores connected in series to a resistance $R_L = 50$ MΩ. The input signals are now the two pH values imposed on the right solutions of the two nanopores, $pH_R = 10.5$ (input 0) and $pH_R = 2.5$ (input 1). The output is the current I_R passing through R_L for $V_L = 2$ V, obtained in each case by solving the electrical circuit of Figure 5b with the experimental nanopore conductances of Figure 3d,e. In previous designs of logic functions with conical nanopores,[4] the logics 0 and 1 were only approximately defined because of the moderate rectification characteristics obtained. The bar charts of Figure 5 demonstrate that the use of cigar-shaped nanopores with improved rectification properties leads to well-defined output signals.

CONCLUSIONS

We have shown experimentally and theoretically that single cigar-shaped nanopores bearing carboxylate groups and amphoteric lysine chains can be operated as resistors and diodes with a broad range of rectifying properties. The nanopore responses can be easily tuned by applying well-defined chemical and electrical signals because of the direct access to the pore mouths in close contact with the external solutions. Other potentially useful characteristics of the new nanopore are the sharp conductance responses (see the $I-V$ curves of Figures 2a,c and 3a,c). These remarkable properties open the door to externally reconfigure single nanostructures in future nanofluidic circuits by using chemical and electrical pulses (see Figure 5), which is most desirable for using the nanopores as chemical processors, transducers, and actuators in controlled release and information processing.

METHODS

Polyethylene terephthalate (PET) membranes of 12 μm thickness (Hostaphan RN 12, Hoechst) were irradiated at the linear accelerator UNILAC (GSI, Darmstadt) with swift heavy ions (Pb, U, or Au) having energy of 11.4 MeV per nucleon. *N*-(3-Dimethylaminopropyl)-*N*′-ethylcarbodiimide hydrochloride (EDC, 98%, Fluka), pentafluorophenol (PFP, 99+%, Aldrich), L-lysine (98+%, Fluka), and copper(II) chloride dihydrate (99%, Merck, Germany) were used as received for the chemical modification. The surfactant Dowfax 2A1 (Dow Chemical) was used as received without further purification. Dowfax 2A1 is an aqueous solution of sodium dodecyl diphenyloxide disulfate.

Fabrication of Single Cigar-Shaped Nanopores. Single nanopores were fabricated in PET membranes irradiated with single swift heavy ions using the surfactant-controlled track-etching technique developed by Apel *et al.*[17] Briefly, the polymer membranes with latent ion tracks were fixed in a sample holder. The etching solution containing 6 M NaOH and 0.06% (v/v) surfactant (Dowfax 2A1, ~45%) was prepared in deionized water and filled in a double-walled etching bath. The temperature of the etching bath was maintained at 60 °C with continuous stirring by circulating heated water through the double walls of the bath. Then, the polymer membranes fixed in the sample holder were immersed in the preheated etching solution. During the whole process, the etching solution was continuously stirred in order to provide a homogeneous etchant concentration in the bath. The etching process was carried out for ~9 min in most of the results presented. After etching, the membranes were taken out from the solution and subsequently dip-rinsed in four beakers containing deionized water separately. For further removal of the residual salts, the etched membranes were additionally immersed in deionized water overnight.

Functionalization of Nanopores. The immobilization of lysine on the pore surface is achieved by means of a previously reported method.[3] The first step is the protection of the α-amino and α-carboxylic groups of the lysine molecule in order to avoid cross-coupling reaction. For this purpose, a solution of L-lysine (50 mM) was prepared in 60% aqueous ethanol (C_2H_5OH/H_2O, 6:4 by volume) and copper chloride (25 mM) was added slowly with continuous stirring. As a result, the blue colored Cu(II) chelate complex of L-lysine was prepared having a free amino group at the terminus of the chain.

The carboxylic (−COOH) groups generated on the pore surface during the track-etching process were modified as follows. First, these groups were converted into pentafluorophenyl esters by using an ethanolic solution of *N*-(3-dimethylaminopropyl)-*N*′-ethylcarbodiimide hydrochloride (EDC, 100 mM) and pentafluorophenol (PFP, 200 mM) for 1 h. Second, the amine-reactive PFP esters were covalently coupled with the ε-amino group of the copper complex of lysine overnight. After being washed with distilled water, the modified pores were exposed to ethylenediaminetetraacetic acid (EDTA, 100 mM) for 2 h in order to remove the copper ions from the surface of the pore. Finally, the modified pore was washed with distilled water thoroughly.

Current−Voltage Measurements. The membrane containing a single (unmodified and modified) nanopore was mounted between the two halves of the conductivity cell filled with a KCl electrolyte solution prepared in a phosphate buffer solution. The pH of the electrolyte was adjusted by dilute HCl or KOH solutions. The Ag/AgCl electrode was placed into each half-cell solution, and a picoammeter/voltage source (Keithley 6487, Keithley Instruments, Cleveland, OH) was used to apply the required voltage. To measure the resulting ion current flowing through the nanopore, a scanning triangle voltage from −2 to +2 V was applied close to the left tip (the solution close to the right tip of the pore remained connected to the ground electrode).

Conflict of Interest: The authors declare no competing financial interest.

Acknowledgment. P.R., J.C., and S.M. acknowledge the financial support from the Ministry of Science and Innovation of Spain, Materials Program (Project Nos. MAT2009-07747) and FEDER. M.A., Q.H.N., S.N, and W.E. gratefully acknowledge financial support by the Beilstein-Institut, Frankfurt/Main, Germany, within the research collaboration NanoBiC, and Prof. C. Trautmann (GSI, Department of Materials Research) for support with irradiation experiments.

Supporting Information Available: Additional experimental results and details of the nanofluidic devices. This material is available free of charge *via* the Internet at http://pubs.acs.org.

REFERENCES AND NOTES

1. Hille, B. *Ion Channels of Excitable Membranes*; Sinauer Associates: Sunderland, 2001.
2. Alcaraz, A.; Ramirez, P.; Garcia-Gimenez, E.; Lopez, M. L.; Andrio, A.; Aguilella, V. M. A pH-Tunable Nanofluidic Diode: Electrochemical Rectification in a Reconstituted Single Ion Channel. *J. Phys. Chem. B* **2006**, *110*, 21205–21209.
3. Ali, M.; Ramirez, P.; Mafe, S.; Neumann, R.; Ensinger, W. A pH-Tunable Nanofluidic Diode with a Broad Range of Rectifying Properties. *ACS Nano* **2009**, *3*, 603–608.
4. Ali, M.; Mafe, S.; Ramirez, P.; Neumann, R.; Ensinger, W. Logic Gates Using Nanofluidic Diodes Based on Conical Nanopores Functionalized with Polyprotic Acid Chains. *Langmuir* **2009**, *25*, 11993–11997.
5. Ali, M.; Ramirez, P.; Tahir, M. N.; Mafe, S.; Siwy, Z.; Neumann, R.; Tremel, W.; Ensinger, W. Biomolecular Conjugation inside Synthetic Polymer Nanopores *via* Glycoprotein–Lectin Interactions. *Nanoscale* **2011**, *3*, 1894–1903.
6. Apel, P. Y.; Blonskaya, I. V.; Didyk, A. Y.; Dmitriev, S. N.; Orelovitch, O. L.; Root, D.; Samoilova, L. I.; Vutsadakis, V. A. Surfactant-Enhanced Control of Track-Etch Pore Morphology. *Nucl. Instrum. Methods Phys. Res., Sect. B* **2001**, *179*, 55–62.
7. Fan, R.; Yue, M.; Karnik, R.; Majumdar, A.; Yang, P. Polarity Switching and Transient Responses in Single Nanotube Nanofluidic Transistors. *Phys. Rev. Lett.* **2005**, *95*, 086607.
8. Harrell, C. C.; Siwy, Z. S.; Martin, C. R. Conical Nanopore Membranes: Controlling the Nanopore Shape. *Small* **2006**, *2*, 194–198.
9. Healy, K.; Schiedt, B.; Morrison, A. P. Solid-State Nanopore Technologies for Nanopore-Based DNA Analysis. *Nanomedicine* **2007**, *2*, 875–897.
10. Lebedev, K.; Mafe, S.; Stroeve, P. Modeling Electrochemical Deposition inside Nanotubes to Obtain Metal-Semiconductor Multiscale Nanocables or Conical Nanopores. *J. Phys. Chem. B* **2005**, *109*, 14523–14528.
11. Murray, R. W. Nanoelectrochemistry: Metal Nanoparticles, Nanoelectrodes, and Nanopores. *Chem. Rev.* **2008**, *108*, 2688–2720.
12. Apel, P. Y.; Blonskaya, I. V.; Orelovitch, O. L.; Ramirez, P.; Sartowska, B. A. Effect of Nanopore Geometry on Ion Current Rectification. *Nanotechnology* **2011**, *22*, 175302.
13. Ramirez, P.; Gomez, V.; Cervera, J.; Schiedt, B.; Mafe, S. Ion Transport and Selectivity in Nanopores with Spatially Inhomogeneous Fixed Charge Distributions. *J. Chem. Phys.* **2007**, *126*, 194703.
14. Ramirez, P.; Apel, P. Y.; Cervera, J.; Mafe, S. Pore Structure and Function of Synthetic Nanopores with Fixed Charges: Tip Shape and Rectification Properties. *Nanotechnology* **2008**, *19*, 315707.
15. Kalman, E. B.; Vlassiouk, I.; Siwy, Z. Nanofluidic Bipolar Transistors. *Adv. Mater.* **2008**, *20*, 293–297.
16. Vlassiouk, I.; Siwy, Z. S. Nanofluidic Diode. *Nano Lett.* **2007**, *7*, 552–556.
17. Apel, P. Y.; Blonskaya, I. V.; Dmitriev, S. N.; Mamonova, T. I.; Orelovitch, O. L.; Sartowska, B.; Yamauchi, Y. Surfactant-Controlled Etching of Ion Track Nanopores and Its Practical Applications in Membrane Technology. *Radiat. Meas.* **2008**, *43*, S552–S559.
18. Hou, Y.; Vidu, R.; Stroeve, P. Solar Energy Storage Methods. *Ind. Eng. Chem. Res.* **2011**, *50*, 8954–8964.
19. Ku, J. R.; Lai, S. M.; Ileri, N.; Ramirez, P.; Mafe, S.; Stroeve, P. pH and Ionic Strength Effects on Amino Acid Transport through Au-Nanotubule Membranes Charged with Self-Assembled Monolayers. *J. Phys. Chem. C* **2007**, *111*, 2965–2973.
20. Karnik, R.; Duan, C.; Castelino, K.; Daiguji, H.; Majumdar, A. Rectification of Ionic Current in a Nanoflidic Diode. *Nano Lett.* **2007**, *7*, 547–551.
21. Sokirko, A. V.; Ramirez, P.; Manzanares, J. A.; Mafe, S. Modeling of Forward and Reverse Bias Conditions in Bipolar Membranes. *Ber. Bunsen.* **1993**, *97*, 1040–1049.
22. Ramirez, P.; Aguilella, V. M.; Manzanares, J. A.; Mafe, S. Effects of Temperature and Ion Transport on Water Splitting in Bipolar Membranes. *J. Membr. Sci.* **1992**, *73*, 191–201.
23. Cheng, L.-J.; Guo, L. J. Entrance Effect on Ion Transport in Nanochannels. *Microfluid. Nanofluid.* **2010**, *9*, 1033–1039.
24. Nguyen, G.; Vlassiouk, I.; Siwy, S. Comparison of Bipolar and Unipolar Ionic Diodes. *Nanotechnology* **2010**, *21*, 265301.
25. Manzanares, J. A.; Kontturi, K.; Mafe, S.; Aguilella, V. M.; Pellicer, J. Polarization Effects at the Cation-Exchange Membrane-Solution Interface. *Acta Chem. Scand., Ser. A* **1991**, *45*, 115–121.
26. Manzanares, J. A.; Mafe, S.; Pellicer, J. Current Efficiency Enhancement in Membranes with Macroscopic Inhomogeneities in the Fixed Charge-Distribution. *J. Chem. Soc., Faraday Trans.* **1992**, *88*, 2355–2364.
27. Kontturi, K.; Murtomäki, L.; Manzanares, J. A. *Ionic Transport Processes*; Oxford University: Oxford, 2008.
28. Ramirez, P.; Rapp, H. J.; Mafe, S.; Bauer, B. Bipolar Membranes under Forward and Rerverse Bias Conditions. Theory *vs.* Experiment. *J. Electroanal. Chem.* **1994**, *375*, 101–108.
29. Cervera, J.; Schiedt, B.; Neumann, R.; Mafe, S.; Ramirez, P. Ionic Conduction, Rectification, and Selectivity in Single Conical Nanopores. *J. Chem. Phys.* **2006**, *124*, 104706.
30. Cervera, J.; Ramirez, P.; Manzanares, J. A.; Mafe, S. Incorporating Ionic Size in the Transport Equations for Charged Nanopores. *Microfluid. Nanofluid.* **2010**, *9*, 41–53.
31. Cervera, J.; Mafe, S. Multivalued and Reversible Logic Gates Implemented with Metallic Nanoparticles and Organic Ligands. *ChemPhysChem* **2010**, *11*, 1654–1658.
32. Manzanares, J. A.; Cervera, J.; Mafe, S. Cooperative Effects Enhance Electric-Field-Induced Conductance Switching in Molecular Monolayers. *J. Phys. Chem. C* **2011**, *115*, 6980–6985.
33. Park, W. I.; Kim, J. S.; Yi, G.-C.; Lee, H.-J. ZnO Nanorod Logic Circuits. *Adv. Mater.* **2005**, *17*, 1393–1397.
34. Cervera, J.; Ramirez, P.; Mafe, S.; Stroeve, P. Asymmetric Nanopore Rectification for Ion Pumping, Electrical Power Generation, and Information Processing Applications. *Electrochim. Acta* **2011**, *56*, 4504–4511.
35. Mafe, S.; Manzanares, J. A.; Ramirez, P. Gating of Nanopores: Modeling and Implementation of Logic Gates. *J. Phys. Chem. C* **2010**, *114*, 21287–21290.